ELSEVIER

Surface Science 402–404 (1998) 401–408

surface science

Stability of two-dimensional clusters on crystal surfaces: from Ostwald ripening to single-cluster decay

Georg Rosenfeld [a,b,*,1], Karina Morgenstern [b,c,2], Ingo Beckmann [b], Wulf Wulfhekel [b,3], Erik Lægsgaard [c], Flemming Besenbacher [c], George Comsa [a]

[a] *Institut für Physikalische und Theoretische Chemie der Universität Bonn, Wegelerstr. 12, D-53115 Bonn, Germany*
[b] *Institut für Grenzflächenforschung und Vakuumphysik, Forschungszentrum Jülich, D-52425 Jülich, Germany*
[c] *Institute of Physics and Astronomy and Center for Atomic-Scale Materials Physics, University of Aarhus, DK-8000 Aarhus, C, Denmark*

Received 25 August 1997; accepted for publication 1 October 1997

Abstract

An overview is given of recent work on the decay of two-dimensional clusters on a Ag(111) surface. Experimental studies using scanning tunnelling microscopy are presented, and various approaches to extract quantitative information on the relevant atomic processes from cluster decay experiments are discussed. It is shown that for typical surface morphologies, the decay rate of individual clusters depends critically on their local environment. Quantitative analysis therefore generally requires complex and detailed case-by-case modelling involving numerical methods. This difficulty can be overcome experimentally by preparing well-defined model structures for which an analytical description can be used without any loss of accuracy.

Keywords: Clusters; Models of surface kinetics; Scanning tunnelling microscopy; Silver; Single crystal surfaces; Surface diffusion; Surface thermodynamics (including phase transitions)

1. Introduction

The decay of two-dimensional clusters or islands plays a key role in coarsening and annealing phenomena of thin crystal films. For a submonolayer film consisting of islands, coarsening may occur through Ostwald ripening, i.e., small islands decay in favour of larger ones. The reason for this well-known phenomenon is the Gibbs–Thomson effect: small islands have a higher vapour pressure than larger islands, and hence there is a net flow of material from small to large islands. Also, the annealing of rough multilayer films involves the decay of individual islands. In a simplified way, a rough multilayer surface may be pictured as stacks of two-dimensional islands, and flattening proceeds via consecutive decay, from top to bottom, of these islands. With the recent advance of methods for direct imaging of crystal surfaces [notably scanning tunnelling microscopy (STM) and low-energy electron microscopy (LEEM)], tools are

* Corresponding author. E-mail: g.rosenfeld@tn.utwente.nl
[1] Present address: Faculty of Applied Physics and Centre of Materials Research, University of Twente, P.O. Box 217, 7500 AE Enschede, The Netherlands.
[2] Present address: Institut de Physique Expérimentale, Université de Lausanne, CH-1015 Lausanne-Dorigny, Switzerland.
[3] Present address: Max-Planck-Institut für Mikrostrukturphysik, Weinberg 2, D-06120 Halle, Germany.

0039-6028/98/$19.00
PII: S0039-6028(98)00024-7

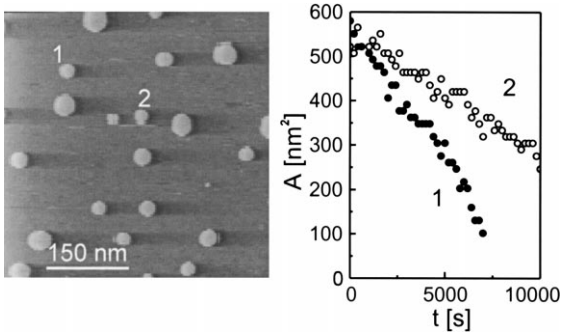

Fig. 1. Left: STM image of Ag adatom islands on Ag(111) at 300 K. Right: area as a function of time for islands labelled 1 and 2.

available for a time-resolved study of these processes, and a number of ''nano-movies'' on cluster decay and related coarsening phenomena have recently been released [1–8].

Whereas it is easy to observe island decay once the imaging method is available, it is not straightforward to interpret these data. A single island measured by a local probe as STM is not the average island described by mean field theories. Any local deviation from the average, e.g. due to the specific local environment of the island studied, may lead to significant changes of the decay behaviour. An example of this statement is given in Fig. 1, showing a typical ensemble of two-dimensional Ag adatom islands on a Ag(111) surface at room temperature. The two islands labelled 1 and 2 have almost the same size, but their neighbourhood is different: the islands in the direct vicinity of island 1 are larger than those in the vicinity of island 2. Due to the Gibbs–Thomson effect, the local adatom density gradient in the vicinity of island 1 is therefore larger than the local gradient near island 2, and hence, island 1 decays significantly faster than island 2 as can be seen from the results shown in the right panel of Fig. 1. A proper quantitative description of particular events observed by STM therefore needs to take the local environment of islands into account, going beyond classical mean field theories on ripening. Similar conclusions have also been reached for ripening of Si islands on Si(100), although the ripening dynamics are different from the case of fcc(111) metals considered here [3,9].

The task of including the local environment can be accomplished using different approaches. One possibility (the most tiresome) is to model in detail the morphology found in the experiment, using as few simplifying assumptions as possible. In general, this requires numerical methods. Another way is to try to map the given surface morphology onto simple geometries for which an analytical model can be used. However, this procedure leads to a good approximation only in a few cases. The third, experimentally demanding but, from our point of view, most elegant approach, is to ''nanofacture'' simple morphologies for which the analytical approach can be used without any further approximation. The present paper will give a short overview of how these different approaches may be realized, and examples will be given from our previous and current work on this topic. Experiments have been performed in Jülich with a room temperature STM of the Besocke-type (Figs. 1 and 4) and in Aarhus with a variable temperature Rasterscope-STM (Figs. 2 and 5) [10,11].

2. Theory of diffusion-limited ripening

We start by formulating the general ingredients needed to model ripening and island decay in a two-dimensional system in the so-called diffusion limit, following the approach described previously [4,12–16]. In this diffusion limit, the mass transport is determined by gradients in the adatom density on the terraces between island edges (or step edges in general) and not by the rate of attachment to island edges. [The latter case leads to the so-called ''interface transfer limit'' and is found for ripening on Si(100) [3].] For metal fcc(111) surfaces, there is generally no additional barrier for attachment of atoms to ascending step edges [17,18], and hence, the diffusion limit applies to ripening on fcc(111) metal surfaces if the atoms diffusing between islands remain on the same terrace level (in other words, diffusing adatoms face only ascending step edges) [4,19]. The task is therefore to solve the (stationary) two-dimensional

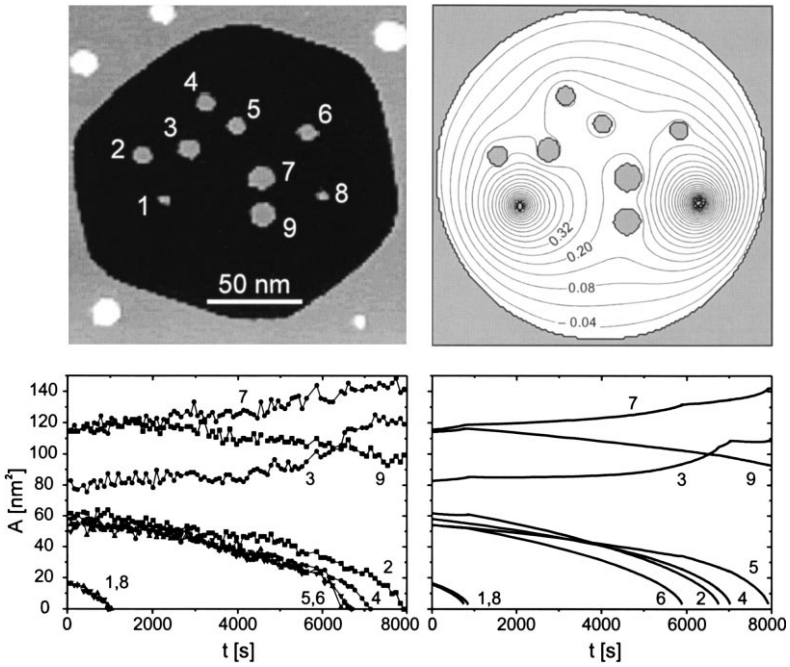

Fig. 2. Upper left: STM image of Ag adatom islands inside vacancy island on Ag(111) at 277 K. Upper right: calculated relative adatom density, $\phi=(\rho-\rho_\infty)/\rho_\infty$, for a morphology modelling the experiment and assuming $\gamma=0.75\,\mathrm{eV\,nm^{-1}}$. The contour lines correspond to constant values of ϕ, the difference between neighbouring lines is $\Delta\phi=0.06$. Lower panels: experimental (left) and simulated (right) decay curves ($\gamma=0.75\,\mathrm{eV\,nm^{-1}}$, $D\rho_\infty=0.05\,\mathrm{s^{-1}}$).

diffusion equation for the adatom density:

$$\Delta\rho=0 \tag{1}$$

in the region between the islands subject to boundary conditions at the island edges. In the direct vicinity of the islands, the adatom density can be assumed to have its equilibrium value prescribed by the Gibbs–Thomson relation [20,21]:

$$\rho_{\mathrm{eq}}(r)=\rho_\infty\exp\left(\frac{\gamma\Omega}{kTr}\right). \tag{2}$$

Here, ρ_∞ is the equilibrium adatom density on a terrace bounded by straight steps, γ is the line tension, Ω is the atomic area, and r is the radius of the respective island, which is assumed to be circular. For monatomic high adatom islands (i.e. two-dimensional crystals) bound by straight steps, the correct formulation of the Gibbs–Thomson relation replaces the radius r by the normal distance h of the side face from the centre of the island (e.g. Ref. [22]). In this paper, we assume for simplicity circular islands and calculate an island radius from the measured island area. For the islands studied here, the difference between h and the radius r calculated in this way is less than 5%. The flux of atoms per unit length, j, into (or away from) the island boundary is given by Fick's first law:

$$j=-D\nabla\rho, \tag{3}$$

where D is the adatom diffusion constant, which, for the examples discussed here (low adatom concentrations), may be taken as the tracer diffusion constant. The total flux of atoms to or from the island boundary, J, is obtained by integrating the atom flux along the island edge. Finally, mass conservation is used: the change of the area, A, of an island is proportional to the total flux of atoms into or away from the island:

$$\frac{\mathrm{d}A}{\mathrm{d}t}=-\Omega J. \tag{4}$$

With these general ingredients, any ripening phenomenon limited by terrace diffusion of single atoms can be modelled. For many experimentally observed morphologies, this requires numerical approaches as used in the following example (cf. Fig. 2).

3. Analysis of experimental results

3.1. Comparison with numerical simulations

We have developed a numerical simulation program that models ripening in the diffusion limit for arbitrary two-dimensional morphologies using an iterative procedure [23]. With each iteration step, the program solves the two-dimensional diffusion equation in the region between island edges, subject to boundary conditions at the island edges where the adatom density is given by the Gibbs–Thomson relation (Eq. (2)). Similar to the approach used in finite-element simulations, the island boundaries are represented by a discrete number of points. The diffusion current into each of these boundary elements is calculated, and with each time step, the element is moved normal to the island boundary (corresponding to an increase or decrease of the island radius) by an incremental amount proportional to the calculated diffusion flux into this boundary element. By varying the decay parameters, which, in the diffusion limit, are the diffusion coefficient $D\rho_\infty$ and the line tension γ (from the combination of Eqs. (2) and (3)), the modelled curves can be fitted to the experimental data.

Fig. 2 presents an example where this approach has been used to describe experimental data. The upper two panels show the initial situation at a substrate temperature of 277 K: on the left, the STM image with nine adatom islands inside a larger vacancy island, and on the right, the calculated adatom density between the islands. The lower two panels show the experimental and modelled decay curves, respectively. For simplicity, during modelling, the border of the large vacancy island is replaced by a circle, and also the adatom islands are assumed to be circular. For the boundary conditions (Eq. (2)), a fixed value of the line tension is chosen: $\gamma = 0.75\ \mathrm{eV\ nm^{-1}}$ as determined earlier [24]. The fitted value of the only remaining free parameter $D\rho_\infty$ amounts to $0.05\ \mathrm{s^{-1}}$ in accordance (within a factor of 1.5) with a more direct determination of this value (see Fig. 5). The overall agreement of the model curves with the experimental results is good. There are, however, details that are not captured correctly, especially for the four islands of starting sizes around $60\ \mathrm{nm^2}$. A better agreement might be obtained by choosing the actual shape of the outer boundary and/or by taking the motion of islands during decay better into account.

3.2. Comparison with analytical solutions

As numerical approaches of this kind are rather tedious, it is better to use analytical solutions of the diffusion problem. To do so, one needs to approximate the island environment by a geometrical boundary at which the adatom density may be specified. The decay problem can then be solved by calculating the diffusion flux between the island boundary and the boundary representing the environment, and for several simple geometries, analytical solutions can be obtained. A simple geometry that is used in classical Ostwald ripening theories is that shown in Fig. 3a: a circular island of radius r surrounded by a circular boundary of radius R. In the mean field theory of Ostwald ripening, this outer boundary is regarded as a locus on the

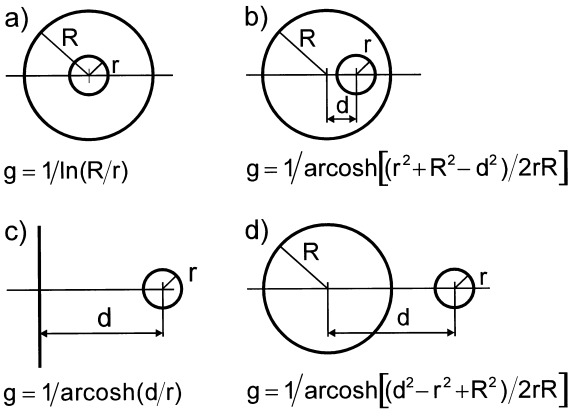

Fig. 3. Geometries for which analytical expressions for the diffusion flux between boundaries can be obtained (see text).

terrace where the adatom density has a value corresponding to the uniform adatom sea produced by all the other islands in the ensemble. The assumption of a uniform adatom sea between the islands is not fulfilled for small systems at finite coverages (i.e. in most experimental cases) as we have seen from the example in Fig. 1: if there were a uniform adatom sea, islands of equal size should have identical decay rates. If the fixed adatom density at this reference boundary is denoted by ρ_0, the particle flux between the island boundary [where the adatom density is $\rho_{eq}(r)$] and the reference boundary is given by:

$$J = 2\pi D g[\rho_{eq}(r) - \rho_0], \quad (5)$$

where we have defined a "geometry function" $g = 1/\ln(R/r)$. However, two concentric circles are only one possible case for which a solution of the two-dimensional Laplace equation can be found. Eq. (5) holds in general also for the flux between an island of radius r and any other boundary at which the adatom density is ρ_0. Some cases for which the diffusion flux can be calculated analytically are sampled in Fig. 3, together with the corresponding geometry function g [25]. These expressions can be used together with Eqs. (2), (4) and (5) to formulate a differential equation for the island area in analytical form. The solution can be fitted to experimental data to estimate the parameters $D\rho_\infty$ and γ.

The inherent difficulty of this approach is the assignment of a reference boundary with uniform adatom density to a given island environment. One possibility is shown in Fig. 4. The small island marked by the arrow on the STM image is surrounded by larger islands of a similar size that do not significantly change in size during the decay of the small island. One may assume that the reference adatom density (ρ_0 in Eq. (5)) for this system is the average equilibrium adatom density of the six islands surrounding the small island, ignoring any possible influence of island further away. This nearest neighbour approach is opposite to the mean-field approach in classical Ostwald ripening theories but probably justified because of the influence of the local environment as already apparent from Fig. 1. Using the appropriate geometry function (Fig. 3b), the decay of the marked island can be modelled. The result is shown in the lower panel of Fig. 4, where we again have set the line tension to a fixed value of 0.75 eV nm^{-1} and have varied only the parameter $D \cdot \rho_\infty$. A good fit is obtained for $D\rho_\infty = 2.0\ s^{-1}$. This value is larger by less than a factor of two than the value determined for the same temperature (304 K) in a more reliable way (see Fig. 5 below).

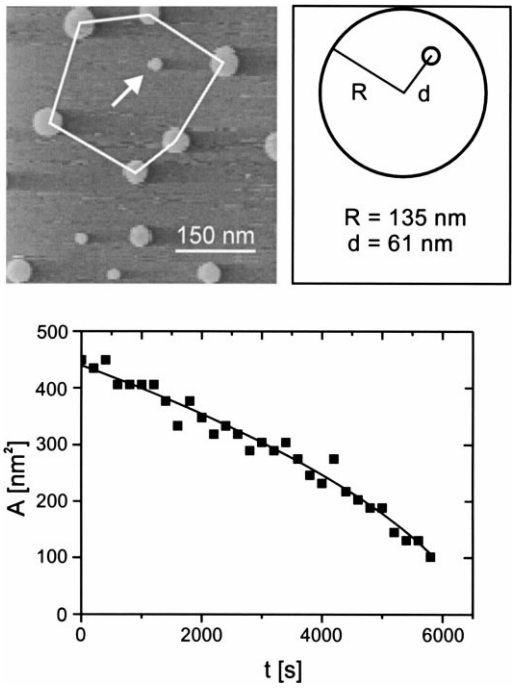

Fig. 4. Modelling of Ag adatom island decay on Ag(111) at 304 K. Upper panels: STM image and model geometry for the marked island. Lower panel: island area as a function of time for the marked island. Squares: experimental data; line: fitted curve using the model geometry indicated above with parameters: $\gamma = 0.75$ eV nm^{-1} and $D\rho_\infty = 2.0\ s^{-1}$.

4. A new approach for quantitative island decay studies

The main disadvantage of the approach of Fig. 4, however, remains the rather ambiguous definition of the outer boundary. A much better way is to prepare morphologies on the surface for which the outer boundary is unambigously defined by an ascending step edge. This can be achieved

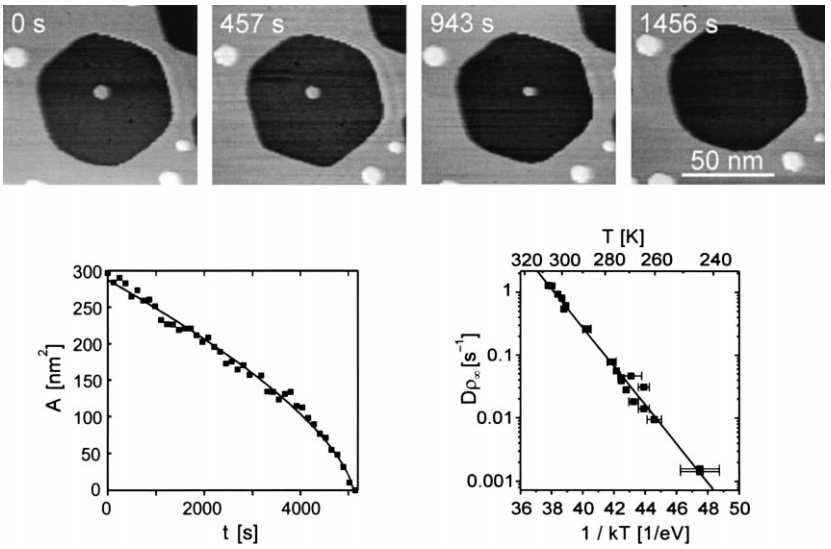

Fig. 5. Ag adatom island decay on Ag(111) in controlled environment. Upper panels: stills of a STM movie showing the decay of an adatom island inside a vacancy island at 277 K. Lower left: example of the fit to a measured decay curve ($T=300$ K). Lower right: temperature dependence of the parameter $D\rho_\infty$ as determined from adatom island decay in vacancy islands for a line tension of $\gamma=0.75$ eV nm^{-1}.

by placing one adatom island into a larger vacancy island (cf. Fig. 5) and, based on previous experience on the control of island densities during homoepitaxy [26], we developed a recipe that can be used to create such structures [24]. The border of the large vacancy island constitutes the outer boundary, and for the adatom density at this boundary (of negative curvature), the equilibrium value according to the Gibbs–Thomson equation (Eq. (2)) can be taken as: $\rho_0=\rho_{eq}(-R)$. These test structures were used for determining the decay parameters of adatom islands by comparing the experimental results to fit curves obtained from Eq. (5) with $g=1/\ln(R/r)$. From data taken at temperatures between 240 K and 310 K, we found that the diffusion coefficient is of the Arrhenius form: $D\rho_\infty=(D\rho_\infty)_0\exp(-E/kT)$ with an activation energy of $E=(0.71\pm0.03)$ eV and a prefactor $(D\rho_\infty)_0=2.5\times10^{11\pm0.6}$ s^{-1} (cf. Fig. 5). In addition, the line tension was estimated to $\gamma=(0.75\pm0.15)$ eV nm^{-1} or, in units of the nearest neighbour distance a_0, $\gamma=(0.22\pm0.04)$ eV/a_0^{-1}.

Within the model used here, the activation energy E corresponds to the sum of the activation energy for adatom diffusion, E_D, and the two-dimensional cohesive energy energy, ΔE, i.e. the energy gained when an adatom is transfered from the terrace to a kink site. The values of the energetic parameters determined are consistent with each other and within the range expected from theoretical estimates. In a simple nearest-neighbour bond model, ΔE corresponds to three nearest-neighbour bonds, whereas the line tension (which must be compared to the energy of steps running in $\langle110\rangle$ directions) corresponds to one nearest-neighbour bond per lattice constant a_0. Substracting a diffusion barrier of 0.1 eV [27] from the measured value of $E=0.71$ eV, we obtain an

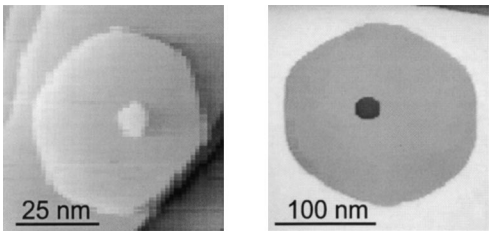

Fig. 6. STM images of model structures on Ag(111) at 300 K. Left: adatom island on adatom island. Right: vacancy island inside vacancy island.

estimate of $\Delta E = 0.61$ eV that is roughly three times the value obtained for $\gamma \cdot a_0$, in line with simple bond counting arguments. Theoretical estimates for Ag(111) are $\Delta E = 0.57$ eV and $\gamma a_0 = 0.19$ eV from the Embedded Atom Method [28], whereas the Effective Medium Theory yields values of $\Delta E = 0.56$ eV and $\gamma a_0 = 0.16$ eV [29]. The agreement with our results is good.

5. Extension to multilevel structures

The main characteristic of model structures like that shown in Fig. 5 is that they represent closed systems containing only one decaying adatom island. Similar closed systems are those of an adatom island on top of another adatom island or a vacancy island inside a vacancy island (cf. Fig. 6). These structures are easier to prepare because they naturally develop during homoepitaxial growth and ion bombardment of surfaces as Ag(111) [or in general fcc(111) surfaces] with a significant barrier opposing downward diffusion at a step edge (step-edge barrier or Ehrlich–Schwoebel barrier). The formalism used so far can be easily extended to include the effect of the step-edge barrier, and here, we will briefly give the result. We define a factor s as the ratio of the diffusion frequency on the flat terrace and that across a descending step: $s = \nu_S/\nu_0 \exp(-E_S/kT)$, where ν_S and ν_0 are the attempt frequencies for step-down diffusion and terrace diffusion, and E_S is the step-edge barrier. For the adatom island on top of another adatom island in concentric geometry, the flux between the two step edges becomes:

$$J = \frac{2\pi D}{\ln(R/r) + a/sR} [\rho_{eq}(r) - \rho_{eq}(R)], \quad (6)$$

where a is the surface lattice constant, and we have assumed that the outer radius R is significantly larger than r ($R > 3r$). In this expression, the reference adatom density ρ_0 (cf. Eq. (5)) is replaced by the adatom density at the lower side of the outer step edge as given by the Gibbs–Thomson relation, i.e. $\rho_0 = \rho_{eq}(R)$ [14,16]. Similarly, for the vacancy island inside the vacancy island in concentric geometry, one obtains [19,16,24]:

$$J = \frac{2\pi D}{\ln(R/r) + a/sr} [\rho_{eq}(r) - \rho_{eq}(-R)], \quad (7)$$

where $\rho_{eq}(r)$ is now the adatom density at the lower side of the inner step edge. Like Eq. (5), these expressions have the form of a rate constant times a concentration difference, but now the expression for the rate constant is more general: besides the term $\ln(R/r)$ from the terrace diffusion part of mass transport, they contain an additional term describing diffusion across the outer and inner step edge, respectively. For $s = 1$, i.e., a vanishing step-edge barrier, the expression for the diffusion-limited case of Eq. (5) is recovered, as $a/R < a/r < \ln(R/r)$. In the other limit of a high step-edge barrier, the logarithm can be neglegted, and the rate constant is proportional to $D \cdot s$. Eqs. (6) and (7) can be used instead of Eq. (5) to model the decay of single adatom islands on top of another adatom islands or vacancy island inside vacancy islands, respectively. The model can also be extended to treat multilevel stacks of adatom islands or multilevel craters yielding a set of coupled differential equations for the area of the different levels in the stack or crater.

6. Conclusions

In summary, we have discussed island decay on metal fcc(111) surfaces using Ag(111) as a model system. Recently, studies on island decay have been extended to the Cu(111) surface with equivalent results [30]. Whereas various ways for a quantitative analysis of experimental data are possible, we believe that the best approach is to produce well-defined nano-structures for which a simple analysis is sufficient to reliably determine decay parameters. The results obtained in this way can then be used as an input for a better understanding of more complex processes such as Ostwald ripening or annealing of rough surfaces.

Acknowledgements

The work at Aarhus was supported by the The Danish National Research Foundation

through the Center for Atomic-scale Materials Physics (CAMP) and the Center for Nanotribology. G.R. acknowledges support from the Deutsche Forschungsgemeinschaft (DFG).

References

[1] D.R. Peale, B.H. Cooper, J. Vac. Sci. Technol. A 10 (1992) 2210.
[2] J.-M. Wen, J.W. Evans, M.C. Bartelt, J.W. Burnett, P.A. Thiel, Phys. Rev. Lett. 75 (1995) 652.
[3] W. Theis, N.C. Bartelt, R.M. Tromp, Phys. Rev. Lett. 75 (1995) 3328.
[4] K. Morgenstern, G. Rosenfeld, G. Comsa, Phys. Rev. Lett. 76 (1996) 2113.
[5] A. Ichiyama, Y. Tanaka, K. Ishiyama, Phys. Rev. Lett. 76 (1996) 4721.
[6] S. Tanaka, N.C. Bartelt, C.C. Umbach, R.M. Tromp, J.M. Blakely, Phys. Rev. Lett. 78 (1997) 3342.
[7] J.B. Hannon, C. Klünker, M. Giesen, H. Ibach, N.C. Bartelt, J.C. Hamilton, Phys. Rev. Lett. 79 (1997) 2506.
[8] W.W. Pai, A.K. Swan, Z. Zhang, J.F. Wendelken, Phys. Rev. Lett. 79 (1997) 3210.
[9] N.C. Bartelt, W. Theis, R.M. Tromp, Phys. Rev. B 54 (1996) 11741.
[10] K. Besocke, Surf. Sci. 181 (1987) 145.
[11] L. Eierdal, F. Besenbacher, E. Lægsgaard, I. Stensgaard, Surf. Sci. 312 (1994) 31.
[12] B.K. Chakraverty, J. Phys. Chem. Solids 28 (1967) 2401.
[13] P. Wynblatt, N.A. Gjostein, in: J.O. McCardin, G. Somorjai (Eds.), Progress in Solid State Chemistry, Vol. 9, Pergamon, Oxford, 1975, p. 21.
[14] J. Villain, Europhys. Lett. 2 (1986) 531.
[15] M. Zinke-Allmang, L.C. Feldman, M.H. Grabow, Surf. Sci. Rep. 16 (1992) 337.
[16] J.G. McLean, B. Krishnamachari, D.R. Peale, E. Chason, J.P. Sethna, B.H. Cooper, Phys. Rev. B 55 (1997) 1811.
[17] G. Ehrlich, Surf. Sci. 331–333 (1995) 865.
[18] R. Stumpf, M. Scheffler, Phys. Rev. Lett. 72 (1994) 254.
[19] G. Rosenfeld, K. Morgenstern, G. Comsa, in: M.C. Tringides, M. Scheffler (Eds.), Surface Diffusion: Atomistic and Collective Processes, NATO ASI-Series, Plenum, New York, 1997, p. 361.
[20] B. Krishnamachari, J.G. McLean, J.P. Sethna, B. Cooper, Phys. Rev. B 54 (1996) 8899.
[21] H. Metiu, G. Rosenfeld, Surf. Sci. 373 (1997) L357.
[22] R. Defay, I. Prigogine, Surface Tension and Adsorption, Longmans Green, London, 1966.
[23] I. Beckmann, W. Wulfhekel, G. Rosenfeld, G. Comsa, Verhandl. DPG (VI) 32 (1997) 872.
[24] K. Morgenstern, G. Rosenfeld, E. Lægsgaard, F. Besenbacher, G. Comsa, Phys. Rev. Lett. 80 (1998) 556.
[25] H.S. Carslaw, J.C. Jaeger, Conduction of Heat in Solids, Clarendon Press, Oxford, 1959.
[26] G. Rosenfeld, N.N. Lipkin, W. Wulfhekel, J. Kliewer, K. Morgenstern, B. Poelsema, G. Comsa, Appl. Phys. A 61 (1995) 45.
[27] H. Brune, K. Bromann, H. Röder, K. Kern, J. Jacobson, P. Stoltze, K. Jacobson, J. Nørskov, Phys. Rev. B 53 (1995) R14380.
[28] R.C. Nelson, T.L. Einstein, S.V. Khare, P.J. Rous, Surf. Sci. 295 (1993) 462.
[29] P. Stoltze, J. Phys. Cond. Mat. 6 (1994) 9495.
[30] G. Schulze-Icking-Konert, M. Giesen, H. Ibach, Surf. Sci., in press.